



*Supplement of*

## **All aboard! Earth system investigations with the CH<sub>2</sub>O-CHOO TRAIN v1.0**

**Tyler Kukla et al.**

*Correspondence to:* Tyler Kukla ([tykukla@colostate.edu](mailto:tykukla@colostate.edu)) and Jeremy K. C. Rugenstein ([jeremy.rugenstein@colostate.edu](mailto:jeremy.rugenstein@colostate.edu))

The copyright of individual parts of the supplement might differ from the article licence.

## S1 Introduction

This supplementary materials document includes further information about the Moist Energy Balance Model, details associated with model stability, a more detailed explanation for the overturning direction of the weathering feedback (see text) and tables with default values and citations for model parameters.

## 5 S2 Moist Energy Balance Model

### S2.1 Details on the Hadley cell parameterization and calculating latent heat flux divergence

Following Siler et al. (2018), we assign a weighting function to partition between Hadley cell (equatorward) and eddy (poleward) latent heat fluxes where the weight ( $w$ ) is defined as:

$$w = 1 - e^{(-x^2/0.3^2)}. \quad (\text{S1})$$

10 Next, the moist static energy flux of the Hadley cell (in  $W$ ) is calculated as a fraction of the total poleward flux ( $F$ ) using the weighting function where:

$$F_{\text{HC}} = (1 - w)F. \quad (\text{S2})$$

We then calculate the total mass transport of the Hadley cell's lower branch ( $\psi$ , in  $kg\ s^{-1}$ , positive southward) from  $F_{\text{HC}}$  by:

$$\psi = \frac{F_{\text{HC}}}{g(x)} \quad (\text{S3})$$

15 where  $g(x)$  is gross moist stability ( $J\ kg^{-1}$ ) and is taken as the difference between upper troposphere moist static energy in the tropics (set at 6% above maximum moist static energy) and near-surface moist static energy  $h(x)$ . This gross moist stability parameterization effectively weakens Hadley circulation in a warmer world. Finally,  $\psi$  is used to calculate  $F_{\text{HC,q}}$  following the main text.

### S2.2 Details on the partitioning of $P$ and $E$

20 To re-iterate from the main text, the equation we use to calculate evaporation ( $E$ ) is Siler et al. (2019)

$$E = \frac{R_G \theta + \rho_{\text{air}} c_p (1 - rh) C_H u}{\theta + \frac{c_p}{L_v q^*}}. \quad (\text{S4})$$

Here, we walk through the parameter values and equations that contribute to this formulation. First,  $R_G$ , with units  $Wm^{-2}$ , is shorthand for the difference between the surface net downward radiative flux ( $R_s$  in Siler et al. (2019)) and the spatial pattern of ocean heat uptake plus heat uptake by frozen hydrometeors at the surface ( $G$  in Siler et al. (2019)). We employ an idealized latitudinal profile for this difference where:

$$R_G = R_s - G = 180 \left[ (1 - x^2) - 0.4e^{-(x/0.15)^2} \right]. \quad (\text{S5})$$

The next term,  $\theta$ , scales the saturation specific humidity ( $q^*$ ) to its change with temperature ( $T$ ) such that

$$\frac{dq^*}{dT} = \theta q^* \quad (\text{S6})$$

where

$$\theta = \frac{L_v}{R_v T^2} \quad (\text{S7})$$

with  $R_v$  being the specific gas constant for water vapor. Relative humidity ( $rh$ ) is set to the global constant value of 80% (Hwang and Frierson, 2010; Siler et al., 2018), although other values or latitudinal spatial profiles of  $rh$  could be easily defined.  $C_h$  is a non-dimensional drag coefficient set to  $1.5 \times 10^{-3}$ . Finally,  $u$  is an idealized spatial profile of the surface wind speed ( $ms^{-1}$ ) defined as:

$$u = 4 + 4 \left| \sin \left( \frac{\pi x}{1.5} \right) \right|. \quad (\text{S8})$$

The idealized formulations for  $R_G$  and  $u$  are held constant for all climate states in this paper, although it would also be reasonable to allow these functions to vary with climate and geography.

### S2.3 Model stability

The equations underlying the MEBM are sensitive to the initial conditions in such a way that certain sets of initial conditions can lead to unexpected results that differ substantially from results that represent very small changes to those initial conditions. For example, figure SS1A shows how the MEBM climate state varies with the temperature boundary conditions. When the temperature guesses for both poles are warm (up and to the right), the model produces an ice-free solution (yellow region) and when both guesses are sufficiently cold the model generates a fully-glaciated ‘‘Snowball’’ solution (gray polygon). Similar

stability maps emerge for other levels of atmospheric  $CO_2$ . As  $CO_2$  decreases sufficiently the multiple stable states collapse  
45 and the both poles (green) solution space expands. We note that this map corresponds to the meridionally-symmetric “Cat-eye”  
geography, and other geographic configurations will have different maps influenced by a number of factors, including how  
symmetric the underlying land and ocean distributions that influence albedo are.

Some pixels in figure SS1A are empty, indicating that the model was unable to find a stable solution within ten seconds.  
This is an arbitrary upper-limit imposed to increase computational efficiency and this limit can be modified by the user. We  
50 have found that if a solution is not reached within ten seconds on a laptop PC it is likely that no solution will be reached and  
the model will time-out after minutes of searching for a solution. The ten-second upper-bound avoids the MEBM stalling in  
these minutes-long null results.

If the model is not solved in ten seconds or it returns a “snowball” solution, a simple set of rules are followed to identify a  
nearby, acceptable solution (the user may also update these rules). Specifically, we search for a new, viable boundary condition  
55 that can be solved in under ten seconds and does not produce a fully-glaciated result. Figure SS1B shows an example of such  
a search. First, the model searches two steps toward a higher N pole temperature guess (marked by arrow 1), then two steps  
toward a higher S pole temperature guess (arrow 2), then indefinite steps with higher N pole temperature guesses until a solution  
is found. Step distance is user-defined (in degrees Celsius). The search stops when the first solution is found. The decision to  
search indefinitely along the N pole temperature axis rather than along the S pole temperature axis is arbitrary but selected to  
60 maintain a simple, reproducible result. We do not move diagonally across the solution space map to minimize the likelihood of  
moving to an ice-free temperature state when the original temperature guesses are proximal to glaciated solutions.

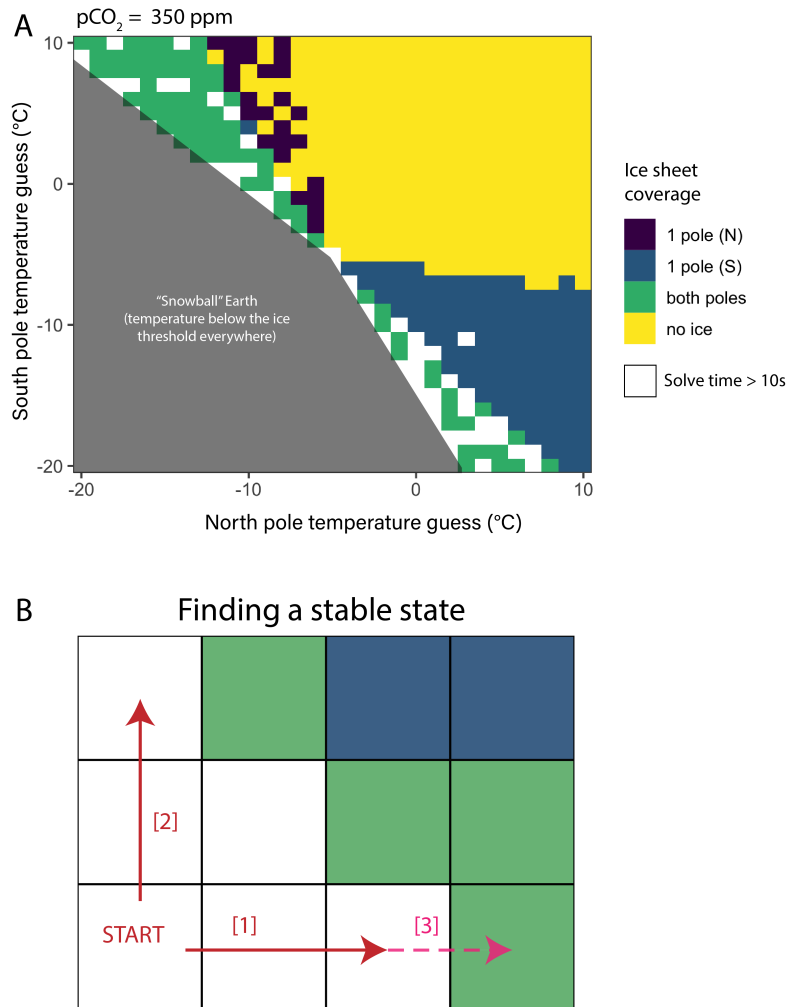


**Figure S1.** (A) Map of climate state (colors) at different temperature guesses (axes) for atmospheric  $p\text{CO}_2$  of 350 ppmv. Warm south and north pole boundary condition temperature guesses give an ice-free solution (yellow), blue and purple represent one glaciated pole, and green is both poles. The gray area to the bottom-left is a “snowball” solution which we deem unreasonable for this work. Blank pixels are where the model took more than 10 seconds to solve. (B) If the model takes longer than 10s to solve or returns a snowball, it looks for an acceptable solution following path [1], then [2], then [3] indefinitely until a solution is reached.

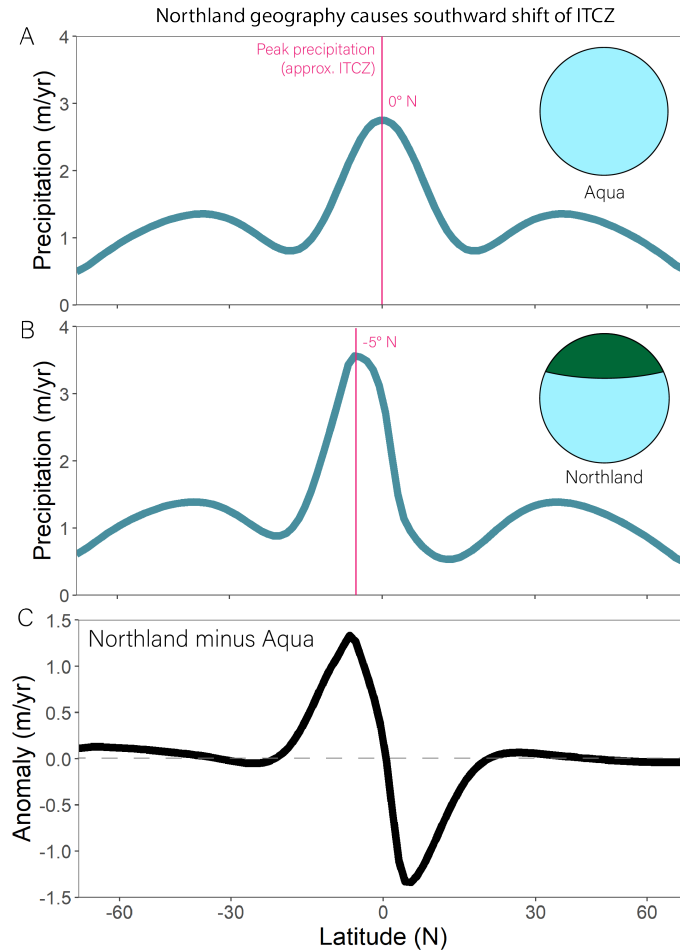


**Figure S2. Precipitation in aquaplanet and Northland configurations.** (A) Aquaplanet mean annual precipitation. Inter-Tropical Convergence Zone (ITCZ) location, defined by peak tropical precipitation, is denoted with magenta line. (B) As (A), but for Northland mean precipitation. (C) Difference between Northland and aquaplanet precipitation.

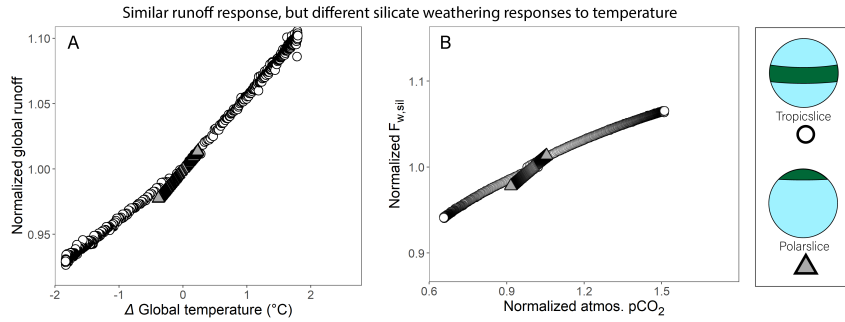


**Figure S3.** (A) Sensitivity of global runoff to temperature. Runoff sensitivity to climate is similar between Tropicslice and Polarslice world. (B) Normalized silicate weathering flux response to  $pCO_2$ . Despite a weaker runoff sensitivity, Polarslice weathering response is similar to Tropicslice world due to polar amplification of warming which compensates for the weaker runoff response.

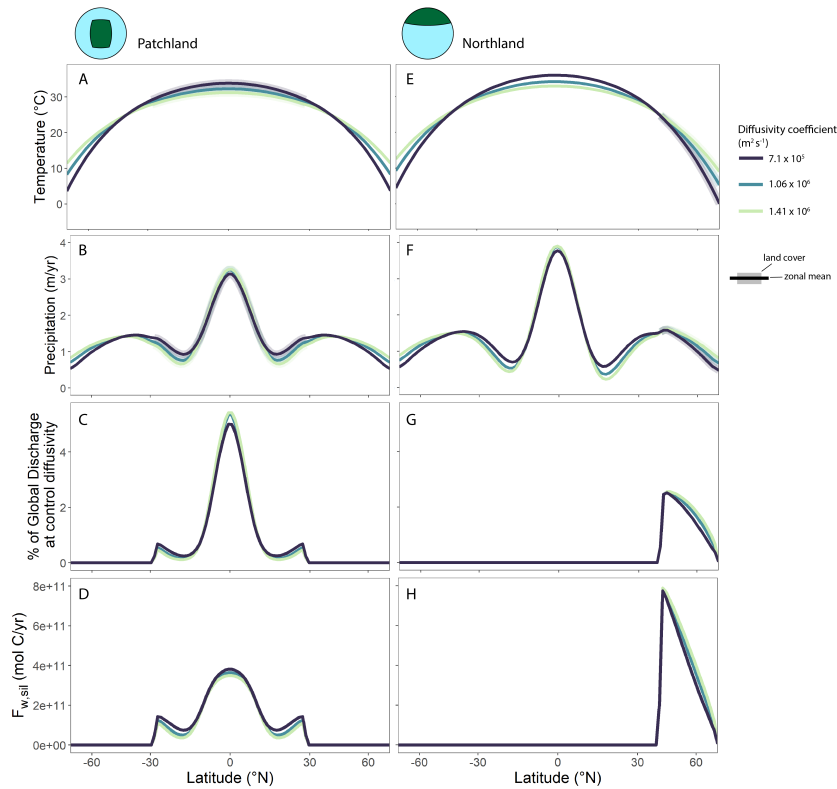


**Figure S4.** Zonal mean climate and weathering in Patchland and Northland. Global temperature (A, E), zonal mean precipitation (B, F), the percent of global discharge (C, G), and the percent of global silicate weathering (D, H) for Patchland world (A-D) and Northland (E-H). Thick, faded line segments in temperature and precipitation panels denote the latitudinal extent of land (whereas discharge and silicate weathering are terrestrial only). Note the trade-off in tropical vs subtropical discharge in Patchland world, leading to temperature-driven changes in weathering driving the climate response.

## References

- Brennan, S. T., Lowenstein, T. K., and Cendon, D. I.: The Major-Ion Composition of Cenozoic Seawater: The Past 36 Million Years from Fluid Inclusions in Marine Halite, *American Journal of Science*, 313, 713–775, <https://doi.org/10.2475/08.2013.01>, 2013.
- 65 Broecker, W. S. and Peng, T. H.: *Tracers in the Sea*, vol. 24, Eldigio Press, Palisades, N.Y., third edn., 1982.
- Caves Rugenstein, J. K., Ibarra, D. E., and von Blanckenburg, F.: Neogene Cooling Driven by Land Surface Reactivity Rather than Increased Weathering Fluxes, *Nature*, 571, 99–102, <https://doi.org/10.1038/s41586-019-1332-y>, 2019.
- Hönisch, B., Hemming, N. G., Archer, D., Siddall, M., and McManus, J. F.: Atmospheric Carbon Dioxide Concentration Across the Mid-Pleistocene Transition, *Science*, 324, 1551–1554, <https://doi.org/10.1126/science.1171477>, 2009.
- 70 Horita, J., Zimmermann, H., and Holland, H. D.: Chemical Evolution of Seawater during the Phanerozoic: Implications from the Record of Marine Evaporites, *Geochimica et Cosmochimica Acta*, 66, 3733–3756, 2002.
- Hwang, Y. T. and Frierson, D. M.: Increasing Atmospheric Poleward Energy Transport with Global Warming, *Geophysical Research Letters*, 37, 1–5, <https://doi.org/10.1029/2010GL045440>, 2010.
- Key, R. M., Kozyr, A., Sabine, C. L., Lee, K., Wanninkhof, R., Bullister, J. L., Feely, R. A., Millero, F. J., Mordy, C., and Peng, T.-H.: A Global Ocean Carbon Climatology: Results from Global Data Analysis Project (GLODAP): GLOBAL OCEAN CARBON CLIMATOLOGY, *Global Biogeochemical Cycles*, 18, n/a–n/a, <https://doi.org/10.1029/2004GB002247>, 2004.
- 75 Kump, L. R. and Arthur, M. A.: Interpreting Carbon-Isotope Excursions: Carbonates and Organic Matter, *Chemical Geology*, 161, 181–198, [https://doi.org/10.1016/S0009-2541\(99\)00086-8](https://doi.org/10.1016/S0009-2541(99)00086-8), 1999.
- Lowenstein, T. K., Timofeeff, M. N., Brennan, S. T., Hardie, L. A., and Demicco, R. V.: Oscillations in Phanerozoic Seawater Chemistry: Evidence from Fluid Inclusions, *Science*, 294, 1086–1088, <https://doi.org/10.1126/science.1064280>, 2001.
- 80 Siler, N., Roe, G. H., and Armour, K. C.: Insights into the Zonal-Mean Response of the Hydrologic Cycle to Global Warming from a Diffusive Energy Balance Model, *Journal of Climate*, 31, 7481–7493, <https://doi.org/10.1175/JCLI-D-18-0081.1>, 2018.
- Siler, N., Roe, G. H., Armour, K. C., and Feldl, N.: Revisiting the Surface-Energy-Flux Perspective on the Sensitivity of Global Precipitation to Climate Change, *Climate Dynamics*, 52, 3983–3995, <https://doi.org/10.1007/s00382-018-4359-0>, 2019.
- 85 Timofeeff, M. N., Lowenstein, T. K., da Silva, M. A. M., and Harris, N. B.: Secular Variation in the Major-Ion Chemistry of Seawater: Evidence from Fluid Inclusions in Cretaceous Halites, *Geochimica et Cosmochimica Acta*, 70, 1977–1994, <https://doi.org/10.1016/j.gca.2006.01.020>, 2006.



**Table S1.** Input parameters and formulas for MEBM component of model.

Long name	Variable	Value or eq'n	units	See equation(s)	Notes	Reference(s)
Earth's radius	$a$	$6.37 \times 10^6$	m	1		
Specific heat of air (constant pressure)	$c_p$	1004	$J kg^{-1} K^{-1}$	2, 6		
Latent heat of vaporization	$L_v$	$2.45 \times 10^6$	$J kg^{-1}$	2, 5	no temperature dependence	
Surface atmospheric pressure	$p_s$	$1.013 \times 10^5$	Pa	3, 4		
Diffusivity coefficient	$D$	$1.06 \times 10^6$	$m^2 s^{-1}$	3, 4	multiply by $\frac{E_a}{y}$ to get kinematic diffusivity	Hwang and Frierson, 2010; Siler et al. 2018
Specific gas constant for vapor	$R_v$	461	$J kg^{-1} K^{-1}$	S7		
Clausius-Clapeyron scaling factor	$\theta$	$\frac{L_v}{R_v T_0^2}$	$K^{-1}$	6		
Near-surface air density	$\rho_{air}$	1.2	$kg m^{-3}$	6		
Relative humidity	rh	0.8		6	bounded [0-1]; global constant	
Bulk transfer coefficient	$C_H$	$1.5 \times 10^{-3}$		6		Siler et al. 2019
Near surface wind speed	$u$	$4 + 4 \left  \sin \left( \frac{\pi z}{100} \right) \right $	$m s^{-1}$	6	idealized zonal mean profile	Siler, pers. comm.
Moisture recycling efficiency	$\omega$	2.6		7	Global mean value	Fu, 1981; Zhang et al. 2004; Greve, 2015
OLR constant (A) intercept	$C_{LW}$	222.5	$W m^{-2}$	10	Often 207 but tuned to higher value for our geographies	Myhre et al. 1998; North and Kim, 2017
OLR constant (A) slope	$M$	18	$W m^{-2}$	10	Often 5.35 but tuned higher for greater clim sensitivity	
Planck feedback sensitivity coefficient	$B$	3.35	$W m^{-2} K^{-1}$	9	Blackbody limit is 4.61	North, 1981; North and Kim, 2017; Koll and Cronin, 2018
Ocean albedo	$\alpha_{ocean}$	0.13			Tunable	
Land albedo	$\alpha_{land}$	0.2			Tunable	
Ice albedo	$\alpha_{ice}$	0.75			Tunable; higher values = stronger ice albedo feedback	
Ice formation threshold	$T_{ice}$	-5	$^{\circ}C$			

**Table S2.** Input parameters and formulas for weathering component of model.

Long name	Variable	Value or eq'n	units	See equation(s)	Notes	Reference(s)
Reactive length scale $\times$ eff. porosity	$L\phi$	0.1	$m$	15		Maher and Chamberlain, 2014
Specific mineral surface area	$A$	0.1	$m^2 g^{-1}$	15		Maher and Chamberlain, 2014
Molar mass	$m$	270	$g mol^{-1}$	15		Maher and Chamberlain, 2014
Global reference temperature	$T_0$	287.15	$K$	16		Maher and Chamberlain, 2014
Theoretical max reaction rate	$r_{max,ref}$	1085	$\mu mol SiO_2 L^{-1} y^{-1}$	16		Maher and Chamberlain, 2014
Activation energy	$E_a$	38	$kJ mol$	17		Maher and Chamberlain, 2014
Init. max equilibrium silicate-derived carbonate	$[C]_{sil,eq}$	374	$\mu mol L^{-1}$	18		Maher and Chamberlain, 2014
Reference reaction rate	$k_{eff,ref}$	$8.7 \times 10^{-6}$	$mol m^{-2} y^{-1}$	16		Maher and Chamberlain, 2014
Soil age	$t_{wz}$	2000	$yr$	15		Maher and Chamberlain, 2014
Max GPP	$GPP_{max}$	$2 \times GPP_0$		20, 21	$GPP_0$ is set to one	Volk, 1989
Minimum $pCO_2$	$pCO_{2,min}$	100	ppmv	20, 21		Volk, 1989; Prentice and Harrison, 2009; Scheff et al. 2017
Land area	$A_{land}$	variable	$m^2$	22	Calculated from input geography file	

**Table S3.** Carbon cycle model inputs.

Long name	Variable	Value or eq'n	units	See equation(s)	Notes	Reference(s)
Initial DIC carbon isotope composition	$\delta^{13}C_i$	0	‰	24		
Volcanism carbon isotope composition	$\delta^{13}C_{vol}$	-5	‰	24		Kump and Arthur (1999)
Carbonate weathering carbon isotope composition	$\delta^{13}C_{carb}$	0	‰	24		Kump and Arthur (1999)
Organic weathering carbon isotope composition	$\delta^{13}C_{org}$	27	‰	24	Defined at first timestep by isotope mass balance.	Kump and Arthur (1999)
Inorganic carbon minus organic carbon isotope composition	$\delta^{13}C_i - \frac{(F_{vol}(\delta^{13}C_{vol} - \delta^{13}C_i) + F_{carb}(\delta^{13}C_{carb} - \delta^{13}C_i) + F_{org}(\delta^{13}C_{org} - \delta^{13}C_i))}{F_{DIC}}$		‰	24	$T_a$ is global mean air temperature	Key et al. (2004)
Mean ocean temperature	$T_o$	$T_a - 10$	°C			Key et al. (2004)
Ocean salinity	(not shown)	35	PSU		Approximation	
Mean ocean pressure	(not shown)	300	bar		Approx. Phanerozoic mean	
Seawater Ca concentration	[Ca]	$15 \times 10^{-3}$	mol L <sup>-1</sup>		Approx. Phanerozoic mean	
Seawater Mg concentration	[Mg]	$48.5 \times 10^{-3}$	mol L <sup>-1</sup>			
Seawater sulfate concentration	[SO4]	$28.2 \times 10^{-3}$	mol L <sup>-1</sup>			
Ocean water volume	(not shown)	$1.4 \times 10^{21}$	L			
Initial ocean pH	$pH_i$	8.2				
Initial volcanic flux	$F_{vol}$	$8 \times 10^{12}$	mol yr <sup>-1</sup>	23, 24, 26, 27		Lowenstein et al. (2001); Breman et al. (2013); Horiata et al. (2002); Timofeeff et al. (2006)
Initial silicate weathering flux	$F_{sil}$	$8 \times 10^{12}$	mol yr <sup>-1</sup>	23, 24, 26, 27		Lowenstein et al. (2001); Breman et al. (2013); Horiata et al. (2002); Timofeeff et al. (2006)
Initial carbonate weathering flux	$F_{carb}$	$12 \times 10^{12}$	mol yr <sup>-1</sup>	23, 24, 25, 27		Broecker and Peng (1982)
Initial carbonate burial flux	$F_{carb}$	$20 \times 10^{12}$	mol yr <sup>-1</sup>	23, 24, 25		Broecker and Peng (1982)
Initial organic carbon weathering flux	$F_{org}$	$8 \times 10^{12}$	mol yr <sup>-1</sup>	23, 24		Key et al. (2004)
Initial organic carbon burial flux	$F_{org}$	$8 \times 10^{12}$	mol yr <sup>-1</sup>	23, 24		Key et al. (2004)